Nanoscale

ROYAL SOCIETY
OF **CHEMISTRY**

PAPER
Colin Lambert, Paul J. Low *et al.*
Exploring relationships between chemical structure and
molecular conductance: from α,ω-functionalised oligoynes
to molecular circuits

NCNST

Check for updates

Exploring relationships between chemical structure and molecular conductance: from α,ω-functionalised oligoynes to molecular circuits†

Elena Gorenskaia,‡[a] Jarred Potter, [ID] ‡[a] Marcus Korb, [ID] [a] Colin Lambert [ID] *[b] and Paul J. Low [ID] *[a]

The quantum circuit rule (QCR) allows estimation of the conductance of molecular junctions, electrode|X-bridge-Y|electrode, by considering the molecule as a series of independent scattering regions associated with the anchor groups (X, Y) and bridge, provided the numerical parameters that characterise the anchor groups (a_X, a_Y) and molecular backbones (b_B) are known. Single-molecule conductance measurements made with a series of α,ω-substituted oligoynes (X-$\{(C\equiv C)_N\}$-X, N = 1, 2, 3, 4), functionalised by terminal groups, X (4-thioanisole (C_6H_4SMe), 5-(3,3-dimethyl-2,3-dihydrobenzo[b]thiophene) (DMBT), 4-aniline ($C_6H_4NH_2$), 4-pyridine (Py), capable of serving as 'anchor groups' to contact the oligoyne fragment within a molecular junction, have shown the expected exponential dependence of molecular conductance, G, with the number of alkyne repeating units. In turn, this allows estimation of the anchor (a_i) and backbone (b_i) parameters. Using these values, together with previously determined parameters for other molecular fragments, the QCR is found to accurately estimate the junction conductance of more complex molecular circuits formed from smaller components assembled in series.

Introduction

Conjugated oligoynes, X-$\{(C\equiv C)_N\}$-X are quintessential examples of molecules with carbon-rich backbones.[1] The electronic structures and physical properties of oligoynes have attracted attention, drawing debate on their suitability as models for the 1D carbon allotrope carbyne.[2,3] In turn, these interests have driven the development and refinement of synthetic methods that allow the preparation of oligoynes terminated by a wide range of stabilising groups.[4] In the rapidly evolving field of molecular electronics, oligoynes functionalised by end-groups that serve as anchors or contacts to secure the molecule within an electrode|molecule|electrode molecular junction are ideally suited for use as wire-like components.[5] The π-conjugated electronic structure of these linear, rigid and length-persistent carbon-rich backbones is not interrupted by aryl rings or bond rotations, as in other wire-like structures, such as those based on oligo(phenylenevinylene) (OPV)[6] and oligo(phenyleneethynylene) (OPE)[7] structures. As a result, current fluctuations across the molecular junction due to conformational changes of the molecule trapped between two electrodes are minimised, whilst the decreasing HOMO–LUMO gap with increasing molecular length results in intriguingly shallow dependence of molecular conductance with length.[8] The rigid structure of oligoynes also leads to low thermal phonon transmission and thermal conductance that decreases with increasing length. When these thermal properties are combined with the relatively high electrical conductance and high Seebeck coefficients of oligoynes that result from charge transport through the tail of the HOMO or LUMO resonances near the Fermi energy and high slope of the transmission function,[9] oligoynes can also be identified as promising molecular materials for thermoelectric applications.[10]

The conceptual construction of oligoynes X-$\{(C\equiv C)_N\}$-Y from a backbone composed of any number of alkyne moieties (N), capped by terminal groups capable of anchoring the molecule to electrode surfaces (X, Y) allows molecular circuits to be fashioned in a manner that highlights simple chemical structure–electrical property relationships. As such, the simplicity of the chemical structures of oligoynes make them ideal objects through which to explore emerging concepts of mole-

[a]*School of Molecular Sciences, University of Western Australia, 35 Stirling Highway, Crawley, Western Australia, 6026, Australia. E-mail: paul.low@uwa.edu.au*

[b]*Department of Physics, University of Lancaster, Lancaster LA1 4YB, England, UK. E-mail: c.lambert@lancaster.ac.uk*

‡Gorenskaia and Potter contributed equally.

cular quantum circuit rules (QCRs),[11–13] that describe the molecular junction as a series of weakly coupled scattering regions, and apply to non-resonant tunnel junctions (*i.e.* those in which the Fermi energy of the electrodes falls near the middle of the transport resonances in the transmission function arising from the HOMO and LUMO). For a molecule of general form X–B–Y (where X and Y are the anchor groups that bind the molecule to the left and right electrodes, and B is the molecular backbone Fig. 1), the QCR writes the conductance of the junction, G_{XBY}, in the form

$$\log\left(\frac{G_{XBY}}{G_0}\right) = a_X + b_B + a_Y \tag{1}$$

where a_X, a_Y and b_B are parameters associated with the moieties X, Y and B respectively. If the independent parameters a_X, a_Y and b_B are known, then eqn (1) allows an algebraic estimate of molecular conductance.[12,14,15]

We report here a systematic study of a series of oligoyne-based molecular wires, $X-(C\equiv C)_N-X$, featuring a range of anchor groups (X = 4-thioanisole (C_6H_4SMe, **1**), 5-(3,3-dimethyl-2,3-dihydrobenzo[*b*]thiophene) (DMBT, **2**), 4-aniline ($C_6H_4NH_2$, **3**), 4-pyridine (Py, **4**)) and composed of different numbers of alkyne moieties in the backbone (*N* = 1 (**a**), 2 (**b**), 3 (**c**), 4 (**d**)) (Chart 1). The single-molecule conductance of each of these compounds, *G*, has been determined using the scanning tunnelling microscope based-break junction (STM-BJ) technique.[16] The trends in molecular conductance across the series have been analysed in relation to the number of alkyne repeat units (*N*) in the backbone and the chemical nature of the anchor group, revealing the expected exponential decay of *G* with *N*. Extrapolation of the ln(*G*) *vs. N* plots to *N* = 0 allows estimates of the conductance of the various anchor groups from experimental data, which in turn can be used to determine the a_i parameters for the anchor groups used in this study. In addition, the experimental data and the algebraic relationships of eqn (1) support further partitioning of the anchor and bridge into a series of smaller scattering regions. Therefore, from the QCR parameters of smaller 'components', estimates of conductance of quite complex molecular 'circuits' can be made (*e.g.* **5–8**, Chart 1). Despite the simplicity of the QCR, these estimates are found to be surprisingly accurate when tested against experimental data.

Fig. 1 A cartoon of a molecular X–B–Y junction with conceptual partitioning into anchor groups (X and Y) and the molecular backbone (B).

Chart 1 Compounds used in this work.

Experimental section

Synthesis of α,ω-functionalised oligoynes

The diarylacetylene (tolan) compounds (Chart 1, *N* = 1, **1a–4a**) were prepared by Sonogashira cross-coupling of the corresponding anchor group functionalised alkyne and aryl-bromide (**2a**) or -iodide (**1a**, **3a**, **4a**).[14,17] The symmetric 1,3-diynes (Chart 1, *N* = 2, **1b–4b**) were prepared by Nevale (**1b**, **2b**),[18] Eglinton (**3b**),[19] or Hay (**4b**)[20] oxidative homo-coupling of the aryl-functionalised alkynes, whilst the asymmetric derivative **5** was prepared by Su–Hay hetero-coupling[21] of 4-ethynylthioanisole with 4-ethynylaniline and isolated in 44% yield after chromatographic separation from the homo-coupled by-products. The hexa-1,3,5-triynes (Chart 1, *N* = 3, **1c–4c**) were prepared by Sonogashira-style cross-coupling of 1,6-bis(triphenylphosphinegold(ɪ))-hexa-1,3,5-triyne[22] with corresponding aryl-functionalised bromide (**2c**) or iodide (**1c**, **3c**, **4c**).[23] The octa-1,3,5,7-tetraynes (Chart 1, *N* = 4, **1d–4d**) were prepared by oxidative homocoupling of terminal buta-1,3-diynes under Su–Hay conditions.[21] The terminal butadiyne reagents that underpin these syntheses were prepared by Su–Hay heterocoupling of the appropriately anchor group functionalised alkyne and 2-methylbut-3-yn-2-ol, followed by deprotection.[24] We note in passing that in contrast to a previous report,[25] the aniline-terminated tetrayne, **3d**, proved to be stable under ambient conditions as a solid, and also as a dilute solution in common solvents. The asymmetrically functionalised oligo(arylene-ethynylene) compounds (**6–8**) were prepared from 4-((4-(methylthio)phenyl)ethynyl)-1-(ethynyl)benzene by Sonogashira coupling

with 4-iodoaniline (**6**) or 9-bromo-10-((4-aminophenyl)ethynyl) anthracene (**8**), or by Su–Hay hetero-coupling with 4-ethynyl-aniline (**7**). Detailed procedures can be found in the ESI.†

Crystallographically determined molecular structures

Interest in the relationships between single molecule conductance and molecular length prompted determination of the molecular structures of **1c**, **1d**, **2d**, **3d**, **4c**, **4d** and **5** by single-crystal X-ray diffraction. Molecular lengths, defined as S···S (**1a–d**, **2a–d**), N···N (**3a–d**, **4a–d**) or S···N (**5–8**), are given in Table 1 from data reported here and elsewhere, and further details of the crystallographic work conducted here, and the resulting molecular and crystal structures, are given in the ESI.†

Conductance measurements

The electrical properties of the compounds in Chart 1 were determined from *ca.* 1 mM solutions in 1,3,5-trimethyl benzene (mesitylene) by scanning tunnelling microscope break-junction (STM-BJ) measurements,[26] conducted with a Keysight 5500 AFM-STM fitted with a log-scale scan head. Sample solutions were introduced into a Teflon liquid STM

cell fitted to a flame-annealed Au-on-glass substrate (Arrandee™). The STM tips were mechanically cut from a length of uncoated Au wire (Goodfellow, 99.999%, 0.25 mm diameter), and the tip and substrate surface tested and analysed by STM imaging of the substrate surface. To collect current–distance traces, the set-point was chosen such that on approach the tip was driven some 2–3 nm into the gold substrate surface, before being retracted at a rate of 5 nm s^{-1} and the tunnelling current recorded. For each compound, 2000 individual traces were recorded under a −100 mV applied bias, with molecular junction formation evinced by plateaus in the otherwise exponential decay of current with tip–substrate separation traces recorded following cleavage of last metal–metal contact.

Results and discussion

Molecular conductance measurements of **1a**, **2a**, and **3a** have been recently described.[14] In this work molecular conductance measurements of **1b–d**, **2b–d**, **3b–d**, **4a–d**, and **5–8** were carried out using the STM-BJ method from solutions of the analyte in

Table 1 Summary of conductivity values of compounds **1a–d**, **2a–d**, **3a–d**, **4a–d**, **5–8**, characteristic lengths, tilt angle θ, junction formation probability (JFP), contact conductance G_{2C}^N, and β^N values

Compound	$\log(G/G_0)^a$	σ^b	$\log(G^{th}/G_0)^c$	$l^{d,e}$ (Å)	L^f (Å)	Δz^{*g} (Å)	$\Delta z^* + z_{corr}{}^h$ (Å)	Tilt angle θ^i (°)	JFP^j (%)	$\ln(G_{2C}^N)^k$	β^N per unit $-(C{\equiv}C)-{}^l$
1a [14]	−3.1 ± 0.1	0.25	−3.13	13.20^d	18.00	6.5	11.5	50.3	100	4.71 ± 0.17	0.55 ± 0.07
1b	−3.25 ± 0.01	0.53	−3.35	15.72^d	20.52	9.1	14.1	55.5	100		
1c	−3.44 ± 0.01	0.54	−3.57	18.33^d	23.13	11.5	16.4	54.7	100		
1d	−3.84 ± 0.01	0.34	−3.92	20.87^d	25.67	13.0	18.0	45.5	100		
2a [14]	−2.7 ± 0.1	0.20	−2.73	13.13^d	17.93	4.5	9.5	58.0	100	5.59 ± 0.1	0.70 ± 0.05
2b	−3.10 ± 0.01	0.40	−2.95	15.66^d	20.46	8.1	12.1	53.7	100		
2c	−3.34 ± 0.01	0.30	−3.17	18.19^e	22.99	11.6	16.6	43.9	100		
2d	−3.74 ± 0.01	0.33	−3.52	20.79^d	25.59	13.3	18.3	44.4	100		
3a [14]	−3.2 ± 0.1	0.40	−3.19	12.48^d	17.28	3.5	8.5	60.5	90	4.60 ± 0.23	0.56 ± 0.09
3b	−3.31 ± 0.01	0.35	−3.41	14.95^d	19.75	6.4	11.4	54.8	90		
3c	−3.57 ± 0.01	0.48	−3.63	17.42^e	22.22	9.2	14.2	50.3	90		
3d	−3.91 ± 0.01	0.40	−3.98	20.08^d	24.88	11.1	16.1	49.7	90		
4a	−3.56 ± 0.01	0.35	−3.47	9.68^d	13.88	4.2	9.2	48.5	90	3.68 ± 0.11	0.53 ± 0.05
4b	−3.77 ± 0.01	0.24	−3.69	12.23^d	16.43	7.5	12.5	40.5	90		
4c	−3.95 ± 0.01	0.39	−3.91	14.82^d	19.02	9.1	14.1	42.2	90		
4d	−4.19 ± 0.01	0.58	−4.26	17.38^d	21.58	12.5	17.5	53.8	90		
5	−3.39 ± 0.01	0.55	—	12.32^e	17.12	5.1	10.1	53.9	100	—	—
6	−4.22 ± 0.01	0.35	—	18.91^e	23.71	8.6	13.6	55.0	80	—	—
7	−4.35 ± 0.01	0.46	—	21.32^e	26.12	14.7	19.7	41.0	100	—	—
8	−4.77 ± 0.01	0.78	—	25.44^e	30.24	19.8	24.8	34.9	100	—	—

^{a} Experimentally determined most probable molecular conductance from STM-BJ measurements in mesitylene; the error range is based on the standard error in the Gaussian fitting of the 1D conductance histograms, reflecting uncertainty in the estimated mean. For different expressions of experimental conductivity (ln(G) and G (nS)) see ESI, Table S1†. ^{b} Standard deviation from the statistical spread of the points forming the conductance histogram peak, indicating distribution of data around the mean. ^{c} Molecular conductance calculated from eqn (1). ^{d} Crystallographically determined S···S or N···N separation. ^{e} S···S or N···N separation determined by Gaussian software. ^{f} The maximum possible length of the corresponding junction ($L = l + 2d$, where d is the distance between the anchor atom and the centre of the contacting gold atom of an idealised pyramidal-shaped electrode: **a** Au–S, $d = 0.24$ nm; **b** Au–S, $d = 0.24$ nm; **c** Au–N, $d = 0.24$, **d** Au–N, $d = 0.21$ nm). ^{g} Experimentally determined break-off distance. ^{h} Break-off distance allowing for snap-back of the gold electrodes (0.5 nm).[28] ^{i} Calculated from $\cos^{-1}((\Delta z^* + z_{corr})/L)$. ^{j} Proportion of current–distance curves containing the featured molecular plateau. ^{k} Conductance of both binding groups, $\ln(G_{2C}^N)$, obtained from the intercept of the $\ln(G)$ *vs.* N plot at $N = 0$. ^{l} The β^N values were obtained from the slope of the plot of conductance *vs.* number units ($N = 1$–4 for **1a–d**, **3a–d**, **4a–d**, and $N = 0$–4 for **2**, **2a–d**) in the molecular backbone (Fig. 2).

mesitylene. As the analyte solution is introduced into the STM liquid cell and the STM tip is brought into position, molecules functionalised with suitable anchor or contact groups assemble on the exposed surfaces of the substrate and tip.[27] The gold STM tip is driven into the gold substrate to create a fused metallic contact. As the tip is retracted, a metallic filament is drawn from the surface which progressively thins as the filament is stretched, evidenced by the decrease in junction conductance in steps corresponding to the quantum of conductance, $G_0 = 2e^2/h = 77.5$ μS. As the metallic junction breaks, the gold contacts snap back *ca.* 0.5 nm,[28] accompanied by a sharp decrease in junction conductance to a value several orders of magnitude less than $1G_0$. In the absence of molecules trapped within the newly opened electrode gap, the junction conductance exponentially decays with tip–substrate distance to the instrument noise floor (which in our case rests between 10^{-5}–$10^{-6}G_0$). However, plateaus in the current *vs.* distance traces with $G \ll G_0$ arise when the newly formed electrode gap is spanned by a molecule and a molecular junction is formed. The molecular geometry within the molecular junction evolves as the tip continues to retract, until the molecule-electrode contact breaks and the junction conductance falls to the noise floor.

Molecular conductance data for **1a–d–4a–d** are summarised in Table 1, with plots of typical conductance (G) *vs.* displacement (s) traces given in Fig. S1–S5.† From these traces, 1D conductance histograms were constructed from all data (*ca.* 2000 traces) with bin width of $\Delta\log(G/G_0)$ of 0.01, and normalised to the number of traces as counts/trace. The 1D histograms display prominent peaks, which are fitted to Gaussian-shaped curves in order to arrive at the most probable conductance values (Table 1). The G *vs.* s data were combined to give 2D conductance-relative displacement heat-maps constructed from all traces, plotted such that the zero displacement coincides with the point of cleavage of the last Au–Au contact in the metallic junction (Fig. S1–S5†).

As would be expected based on a simple tunnelling model, for each series of compounds with the same anchor group, and for data collected in the same solvent to avoid convoluting the effects of tunnel length with solvent gating phenomena,[29] the conductance features shift to lower values as the number of C≡C moieties, and hence the molecular length, increases *i.e. G***Xa** > G**Xb** > G**Xc** > G**Xd** (Table 1). The single molecule conductance is also found to depend on the anchor group, with the DMBT-functionalised compounds giving rise to higher conductance than the comparably structured members of the thioanisole, aniline or pyridine family (Table 1). Both features are clearly revealed by the 2D heat maps, with the high data density regions shifting to lower conductance regions with increasing relative displacement, and trending with the anchor group (**i** = **a–d**) such that G **2i** > **1i** > **3i** > **4i**.

The rigid, linear structure of oligoynes and homologous chemical structure of the backbone makes compounds such as **1a–d–4a–d** ideal for studies of molecular junction conductance *vs.* length dependence, the number of alkyne repeat units and the nature of the anchor group.[1,8,25,30,31] From a tunnelling

model, the molecular conductance (G) is expected to display an exponential decay with junction length, L, according to the relationship

$$G = G_{2C}e^{-\beta L} \tag{2}$$

where G_{2C} is an effective contact conductance that combines contributions from both the left and right anchor-electrode contacts. The decay (or attenuation) constant β describes the electronic properties of the bridge as a function of length (eqn (2)).

The linear fit of conductance *vs.* length data according to eqn (2) has often been used to explore and test coherent tunnelling transport models of molecular conductance for various combinations of anchor group and molecular backbones. However, the correlation of the experimentally determined break-off distance (after allowing for the electrode snap-back) which corresponds to the tip–substrate separation at point of cleavage of the molecular junction and the charge transport distance through the length of the molecule is convoluted by the contact angle imposed by the chemical nature of the interaction between the anchor group and the electrode surface(s) (Fig. S6† and Table 1). The transport distance L (*i.e.* the length of the tunnel barrier represented by the geometry of the molecular junction) is therefore often estimated as the crystallographically determined or geometry optimised distance between the anchor atoms, l. Some authors have suggested that the true junction length should also include the anchor atom – gold distance, d (*i.e.* $L = l + 2d$), where for the anchor groups used here, $d = 0.24$ nm (series **1**, Au-SMe;[32] series **2**, Au-(S) DMBT;[32] series **3**, Au-NH$_2$[25]) or 0.21 nm (series **4**, Au-(N)Py;[25] Table 1). Regardless of the method of estimation, the transport distance necessarily reflects the structures of both anchor groups and the bridge. Therefore, the decay parameter β reflects the specific combination of anchor group and backbone structure in the molecular series under investigation, and given this term is also solvent dependent,[29] it has limited use as a predictive or design tool.

Alternatively, structure–property relationships contained in the conductance data can be interpreted not as a function of junction length, but in terms of the number of repeat units in the molecular backbone, N. In this description, eqn (2) is re-expressed as

$$G = G_{2C}^N e^{-\beta^N N} \tag{3}$$

In eqn (3), the β^N values reflect conductance decay per repeat unit in the bridge (*i.e.* the number of –{C≡C}– moieties in the case of the oligoynes **1–4**, N) whilst G_{2C}^N reflects the inherent conductance through both anchor groups in the junction in contact with the electrodes (as distinct from G_{2C} which describes the conductance through the two anchor atom-gold contacts). For the compounds **1a–d–4a–d**, the attenuation factors β^N (determined from the slope of a linear fit to the ln (G) *vs.* N data, Fig. 2) are determined to be 0.55 per unit (series **1**, C$_6$H$_4$SMe anchors), 0.70 per unit (series **2**, DMBT anchors), 0.56 per unit (series **3**, C$_6$H$_4$NH$_2$ anchors), and 0.53 per unit
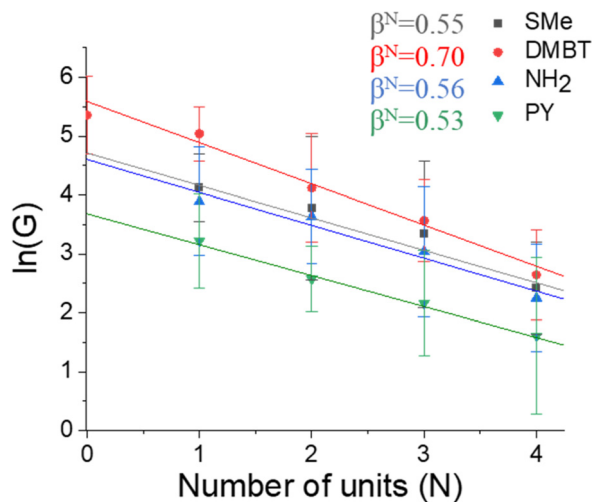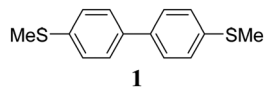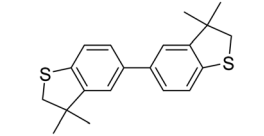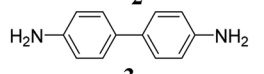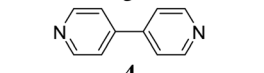
Fig. 2 Plot of the most probable experimental conductance values ln (*G*) *versus* number of units −{C≡C}−, *N*, from STM-BJ measurements in mesitylene.

(series **4**, Py anchors) in mesitylene. These values are consistent with the range of previously reported decay constants of oligoynes featuring various anchor groups,[1,8,25,29,31] and back calculation gives excellent agreement with the individually determined experimental conductance values (Table S2 and Fig. S7†).

The term associated with molecular conductance through both anchor groups (G_{2C}^N) can be obtained from an extrapolation of the ln(*G*) *versus* N plots to N = 0 (Fig. 2 and Table 1). In the present context, the conductance at N = 0 (*i.e.* $G = G_{2C}^N$) reflects the molecular conductance of the biaryl compounds 4,4′-bis(methylthiol)biphenyl (**1**),[33–36] 5,5′-bis(3,3-dimethyl-2,3-dihydrobenzo[*b*]thiophene) (**2**, this work, Fig. S8 and Table S3†), 4,4′-diaminobiphenyl (**3**),[36,37] and 4,4′-bipyridine (**4**).[38–41] Indeed, the values of G_{2C}^N obtained from extrapolation are in excellent agreement with the available experimental molecular conductance data from the authentic biaryl compounds **1**–**4** (Table 2). The decay parameter, β^N, and the conductance term, G_{2C}^N, provide metrics that describe the properties of the bridge and the left and right anchor groups, respectively. As values for β^N and G_{2C}^N can be evaluated from the slope and intercept of a linear plot of ln(*G*) *vs.* N constructed from a small number of experimental measurements, eqn (3) allows, in principle, the molecular conductance of any member of a homologous series of wire-like molecules to be determined in a given solvent, assuming there is no change in conductance mechanism for the bridge length considered.[42–44]

The quantum circuit rule (eqn (1)) provides a complementary approach to rationalising structure–property relationships in oligoyne molecular wires and predicting conductance properties from independent and transferrable parameters associated with the anchor (a_X, a_Y) and bridge (b_B) components that, together, comprise the molecular structure (Table 3 and Fig. 3).[12]

Table 2 Experimental conductivity of 4,4′-bis(methylthiol)biphenyl, 5,5′-bis(3,3-dimethyl-2,3-dihydrobenzo[*b*]thiophenyl), 4,4′-diaminobiphenyl and 4,4′-bipyridine in mesitylene, the contact group conductance term from extrapolation of Fig. 2 to N = 0 expressed as log(G_{2C}^N/G_0) (see also Table S4†), and twice the value of the quantum circuit rule anchor parameter for each anchor group, $2a_X$,[12,14,15] for ease of comparison

Compound	log(G/G_0) (solvent)[a]	log(G_{2C}^N/G_0)	$2a_X$
MeS—⬡—⬡—SMe **1**	−2.80 (TCB)[33] −2.90 (TCB)[34] −2.89 (TCB)[35] −2.75 (TCB)[36] −2.56 (TMB)	−2.84 −2.46	−2.82 −2.42
2			
H_2N—⬡—⬡—NH_2 **3**	−2.95 (TCB)[36] −2.85 (TCB)[37]	−2.89	−2.88
N⬡—⬡N **4**	−3.30 (TCB)[38] −3.30 (unknown)[39] −3.35 (TCB)[40] −3.30 (TCB)[41]	−3.29	−3.16

[a] Experimentally determined single molecule conductance (TCB = 1,2,4-trichlorobenzene; TMB = 1,3,5-trimethylbenzene (mesitylene)).

In order to determine or verify the various anchor group parameters, a_X, it is helpful to consider the polyyne molecules **1a–d**–**4a–d** in terms of the general structural description X-(C≡C)$_N$-X, where N has the usual meaning of number of C≡C repeat units and X represents the anchor group (X = 4-thioanisole (C_6H_4SMe, **1**), 5-(3,3-dimethyl-2,3-dihydro benzo[*b*]thiophene) (DMBT, **2**), 4-aniline (C_6H_4NH$_2$, **3**), 4-pyridine (Py, **4**)). In the case N = 0 described above (*i.e.* $b_B = 0$) the QCR (eqn (1)) predicts

$$\log\left(\frac{G_{2C}^N}{G_0}\right) = \frac{\ln\left(\frac{G_{2C}^N}{G_0}\right)}{\ln 10} = 2a_X \qquad (4)$$

There is excellent agreement between the experimentally determined values of molecular conductance of the biaryls X–X (**1**–**4**, Table 2), the previously determined anchor parameters, a_X (Table 3), and the value obtained from extrapolation of the data shown in Fig. 2 (Table 2). This excellent agreement between experiment and the predictions of the QCR is no doubt due in part to the non-planar structure of biaryls, which limits conjugation between the two rings and allows approximation of the structure as two weakly coupled scattering sites.

From the QCR (eqn (1)), the a_X parameters (Table 3) and the experimental conductance data presented as log(G/G_0) (Table 1), the backbone parameters, b_B, for the various homologous members of the polyyne series investigated here ($b_{C≡C}$, $b_{C≡CC≡C}$, $b_{C≡CC≡CC≡C}$ and $b_{C≡CC≡CC≡CC≡C}$) are readily calculated (Table 3); these values differ slightly from those derived earlier from studies of related series,[12] but each

Table 3 Quantum circuit rule parameters, a_X, for anchor groups and b_B for backbones used in this work[12,14,15]

Anchor group	C$_6$H$_4$SMe	DMBT	C$_6$H$_4$NH$_2$	Py
a_X [12,14]	−1.41	−1.21	−1.44	−1.58
Backbone	**a**	**b**	**c**	**d**
b_B [12]	−0.31 ± 0.09	−0.63 ± 0.03	—	−1.20 ± 0.07
b_B this work	−0.31 ± 0.09 [12]	−0.53 ± 0.11	−0.75 ± 0.11	−1.1 ± 0.13
Backbone				
b_B [15]	−1.37		−1.03	−0.74
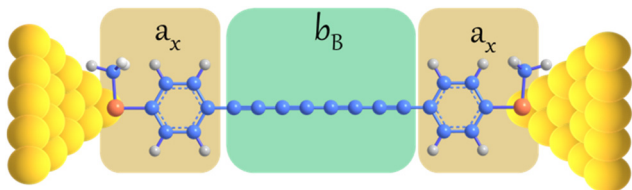
Fig. 3 A simple schematic of a molecular junction formed from **1d**, illustrating the conceptual partitioning of the molecule into anchor groups and backbone components.

set of parameters employed with eqn (1) give remarkably good agreement with the experimentally determined conductance values.

Since the QCR treats each region of the molecule as an independent scattering region, an alternative analysis of the data can be made by incorporating the anchor groups within the scattering region associated with the junction electrode, and considering the conductance due to the (arbitrarily partitioned) bridge portion alone (Fig. 4).
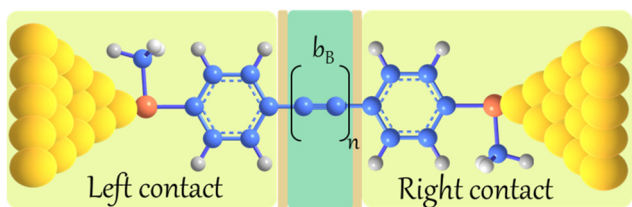
Fig. 4 Schematic illustration of incorporating the anchor groups within the electrode scattering region.

In such a model, the Simmons-like eqn (3) for molecules in which the backbone is composed of a homologous series of N molecular repeat units (*i.e.* such as **1a–d–4a–d**) allows an expression for conductance of the bridge, G_B, to be written

$$G_B = G_{2B}^N e^{-\beta_B^N N} \tag{5}$$

where β_B^N is a decay parameter per unit of the bridge that is independent of the anchor group, and G_{2B}^N is a contact parameter, discussed further below. Furthermore, from the QCR, the conductance of this modified junction can be written simply as

$$\log\left(\frac{G_B}{G_0}\right) = b_B \tag{6}$$

allowing G_B to be evaluated for each backbone fragment for which the bridge parameter is known. For example, given the b_B values of the various –{(C≡C)$_N$}– backbones determined above and summarised in Table 3 it is possible to calculate G_B for each chain length from eqn (6), and hence plot the linear relationship of $\ln(G_B)$ *vs.* N predicted from eqn (5) (Fig. 5). The slope of the $\ln(G_B)$ *vs.* N plot gives $\beta_B^N = 0.60$ per C≡C moiety, in good agreement with the average values obtained for each series **1a–d–4a–d** (Fig. 2). In principle, such plots of $\ln(G_B)$ *vs.* N can be extrapolated or interpolated to arrive at bridge parameters (b_B) for members of a homologous series from the often limited available experimental conductance data or derived b_B parameters.

The $\ln(G_{2B}^N)$ term obtained as the intercept at $N = 0$ in Fig. 5 represents the conductance through the contacts between backbone and the modified electrode through the two C$_{sp}$–C$_{sp^2}$ bonds (beige shaded regions of Fig. 4). From Fig. 5, the
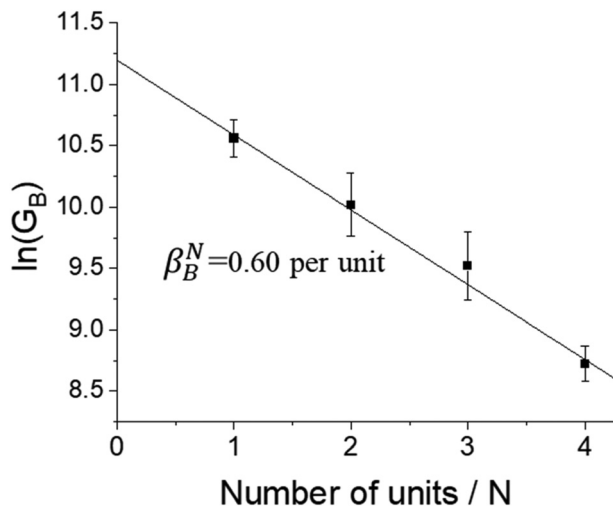
Fig. 5 Plot of the most probable experimental conductance values of backbone $\ln(G_B)$ versus number of units.

Fig. 6 Plot of the most probable experimental conductance values ln (*G*) of MeS{(C$_6$H$_4$)$_N$}SMe and H$_2$N{(C$_6$H$_4$)$_N$}NH$_2$,[36] versus number of *para*-phenylene units −C$_6$H$_4$−, N.

numerical value of the intercept ($\ln(G_{2B}^N) = 11.20$) gives $G_{2B}^N = 73\,130$ nS, very close to quantum conductance ($G_0 = 73\,480$ nS) supporting the effective partitioning description of Fig. 4.

The QCR (eqn (1)) has immense potential for use in molecular circuit design, giving a simple algebraic expression that can estimate single-molecule conductance with surprising accuracy should the unique numerical parameters be known for the particular anchor group(s) (a_X, a_Y) and bridge structure (b_B) in the molecule of interest. The strategies outlined above provide convenient methods to estimate these terms from a small set of experimental data. With a view to developing a bigger library of transferrable parameters associated with smaller fragments and further exploring the application and limits of the QCR, attention is now turned to oligo(phenylene) compounds, MeS-{(C$_6$H$_4$)$_N$}-SMe and H$_2$N{(C$_6$H$_4$)$_N$}NH$_2$, for which experimentally determined molecular conductance values are known (Table 4).[36] From these data, treating the SMe or NH$_2$ groups as the anchors and the oligo(*para*-pheny-

lene) moiety as the 'bridge' permits an analysis of molecular conductance (as $\ln(G)$) *vs.* number of phenylene rings, similar to that described in Fig. 2 to be conducted (Fig. 6). The intercept of the linear plots shown in Fig. 6 at $N = 0$ gives values ln (G_{2C}^N) corresponding to the contact conductance of the very short compounds dimethyldisulfide (MeSSMe) and hydrazine (H$_2$NNH$_2$), which would be extraordinarily challenging to measure directly and from which the anchor parameters of the individual thiomethyl (a_{SMe}) and amine (a_{NH_2}) groups can be determined (eqn (4) and Table 5).
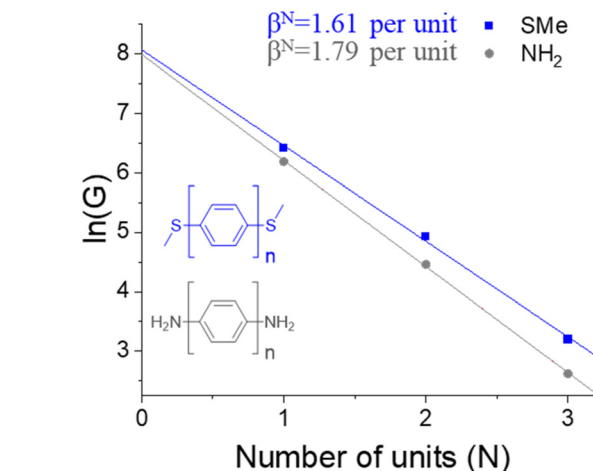
To assess the bridge parameter associated with the *para*-phenylene moiety, a common 'component' of many molecular circuits, recall that the QCR begins by treating the molecular structure as a series of independent scattering regions, arbitra-

Table 5 Conductance terms G_{2C}^N obtained from the intersection of most probable experimental conductance values ln(*G*) of MeS{(C$_6$H$_4$)$_N$}SMe and H$_2$N{(C$_6$H$_4$)$_N$}NH$_2$,[36] at $N = 0$, and a_i

Anchor group	$\ln G_{2C}^N$	G_{2C}^N (nS)	$\log(G_{2C}^N/G_0)$	a_i [a]
–SMe	8.07	3197.1	−1.38	−0.69
–NH$_2$	7.99	2951.3	−1.42	−0.71

[a] From eqn (4).

Table 4 Experimental conductance values of −SMe and −NH$_2$ anchored oligo(*para*-phenylene) compounds[36]

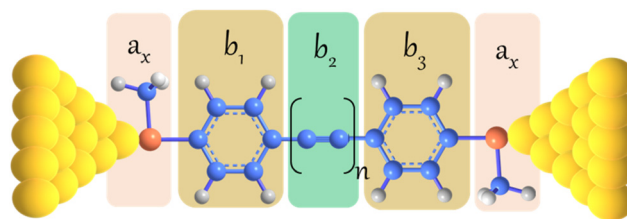| Compound	$\log(G/G_0)$	G (nS)	$\ln(G)$
MeS⬡SMe	−2.10	615.4	6.42
MeS⬡⬡SMe	−2.75	137.8	4.93
MeS⬡⬡⬡SMe	−3.50	24.5	3.20
H$_2$N⬡NH$_2$	−2.20	488.9	6.19
H$_2$N⬡⬡NH$_2$	−2.95	86.9	4.46
H$_2$N⬡⬡⬡NH$_2$	−3.75	13.8	2.62

Fig. 7 Partitioning of thioanisole-anchored polyynes into anchors and subdivided backbone.

Fig. 8 Schematics of compounds **5–8** illustrating various partitioning strategies dividing the molecule into separate 'components' of the anchor groups and backbone fragments for which a_i and b_B parameters are known, assembled in series, the resulting calculated conductance values (log(G^{th}/G_0)) from the QCR (eqn (7)) and experimentally determined values from STM-BJ measurements (log(G^{exp}/G_0)).

rily partitioned as 'anchor' or 'bridge' regions, with the overall conductance given by the sum of the unique and transferrable parameters associated with each of these regions (eqn (1)). It follows that for a more complex molecular structure that can be partitioned into a number of smaller scattering regions, eqn (1) might be usefully re-expressed as

$$\log\left(\frac{G}{G_0}\right) = \sum a_i + \sum b_i \qquad (7)$$

The oligo(*para*-phenylene) backbones in MeS$\{(C_6H_4)_N\}$SMe and $H_2N\{(C_6H_4)_N\}NH_2$, present as an ideal case of a bridge composed of a number of independent scattering regions and as such we can write for the SMe-anchored compounds series of Table 4

$$\log\left(\frac{G}{G_0}\right) = 2a_{SMe} + Nb_{C_6H_4} \qquad (8a)$$

and analogously for the NH_2-anchored compounds

$$\log\left(\frac{G}{G_0}\right) = 2a_{NH_2} + Nb_{C_6H_4} \qquad (8b)$$

Average solutions for $b_{C_6H_4}$ using the data in Table 4 from the SMe (eqn (8a), $b_{C_6H_4} = -0.71$) and NH_2 series (eqn (8b), $b_{C_6H_4} = -0.77$) are comparable, leading to a proposed value of $b_{C_6H_4} = -0.74$ (Table 3). Pleasingly, the sum of a_{SMe} (−0.69) or a_{NH_2} (−0.71) and $b_{C_6H_4}$ (−0.74) are close to the previous estimates of the aryl anchor parameter $a_{C_6H_4SMe}$ (−1.41) and $a_{C_6H_4NH_2}$ (−1.44). Consequently, if one considers the anchors and backbones in molecules partitioned as shown in Fig. 7 for **1a–d**, by way of example, and applies eqn (7) using the parameters in Tables 3 and 5, excellent agreement with experiment is also achieved (Table S2†).

To more rigorously test the approach described by eqn (7), a series of 'modular' molecular circuits (**5–8**) have been designed, with various chemical 'components' assembled in series in such a way that a variety of partitioning strategies are possible and feature different anchors at each terminus (Fig. 8). For each of these partitioning conditions, the single-molecule conductance has been estimated from eqn (7) and the various a_i and b_i parameters summarised above. The accuracy of these estimates ($\log(G^{th}/G_0)$) can be tested against the single-molecule conductance of authentic samples measured using STM-BJ methods (Table 1 and Table S1†). As summarised in Fig. 8, the algebraic 'circuit rule' approach allows the estimation of conductance through these rather complex molecules with a remarkable degree of accuracy.

Conclusion

In this work α,ω-substituted oligoynes (X-$\{(C\equiv C)_N\}$-X, N = 1, 2, 3, 4) functionalised by anchor groups, X (4-thioanisole (C_6H_4SMe), 5-(3,3-dimethyl-2,3-dihydrobenzo[*b*]thiophene) (DMBT), 4-aniline ($C_6H_4NH_2$), 4-pyridine (Py) have been synthesised and characterised. To address the individual molecule

conductance of polyynes, the scanning tunnelling microscope break junction (STM-BJ) technique has been used. The experimental study has shown that conductance decreases in an exponential manner with molecular length and hence also with the increase in number of repeat units –(C≡C)– in a molecule. The β^N values that reflect conductance decay per unit in the bridge are determined to be 0.55 per unit (series **1**, C_6H_4SMe), 0.70 per unit (series **2**, DMBT), 0.57 per unit (series **3**, $C_6H_4NH_2$), and 0.53 per unit (series **4**, Py) in mesitylene. Molecular conductances through both anchor groups (G_{2C}^N) have been obtained from extrapolation of $\ln(G)$ *versus* N plots to N = 0 for polyynes with different anchor groups. The G_{2C}^N term reflects the molecular conductance of the biaryl compounds (4,4′-bis(methylthio)biphenyl, **1**; 5,5′-bis(3,3-dimethyl-2,3-dihydrobenzo[*b*]thiophene), **2**; 4,4′-diaminobiphenyl, **3**; and 4,4′-bipyridine, **4**) and supported by experimental conductance measurements of corresponding compounds.

Further application of the quantum circuit rule (QCR) allows estimation of the conductance of molecular junctions by considering the molecule as a series of independent scattering regions with corresponding numerical parameters associated with the anchor groups (a_i) and molecular backbones (b_i). Results from this method of analysis have shown excellent agreement with the experimentally determined data. Also, the exponential dependence of molecular conductance with the number of repeating –(C≡C)– units allows experimental estimates of the anchor and backbone parameters. Furthermore, the QCR was verified for a series of 'modular' molecular circuits by applying a variety of partitioning strategies allowing subdivision of anchor groups and backbones on circuits into smaller components assembled in series with known numerical parameters. Estimated results for complex molecules are well-supported by experimentally determined molecular conductances. The fact that the QCR can predict molecular conductance with high accuracy allows the electrical conductance of future molecules to be predicted, ahead of their synthesis and demonstrates that the QCR is a useful design tool for molecular-based electronic devices.

Conflicts of interest

There are no conflicts to declare.

Acknowledgements

References

1 M. Gulcur, P. Moreno-García, X. Zhao, M. Baghernejad, A. S. Batsanov, W. Hong, M. R. Bryce and T. Wandlowski, *Chem. – Eur. J.*, 2014, **20**, 4653–4660.

2 D. Prenzel, R. W. Kirschbaum, W. A. Chalifoux, R. McDonald, M. J. Ferguson, T. Drewello and R. R. Tykwinski, *Org. Chem. Front.*, 2017, **4**, 668–674.

3 W. A. Chalifoux and R. R. Tykwinski, *Nat. Chem.*, 2010, **2**, 967–971.

4 W. A. Chalifoux and R. R. Tykwinski, *C. R. Chim.*, 2009, **12**, 341–358.

5 M. R. Bryce, *J. Mater. Chem. C*, 2021, **9**, 10524–10546.

6 H. Liu, N. Wang, J. Zhao, Y. Guo, X. Yin, F. Y. C. Boey and H. Zhang, *ChemPhysChem*, 2008, **9**, 1416–1424.

7 V. Kaliginedi, P. Moreno-García, H. Valkenier, W. Hong, V. M. García-Suárez, P. Buiter, J. L. H. Otten, J. C. Hummelen, C. J. Lambert and T. Wandlowski, *J. Am. Chem. Soc.*, 2012, **134**, 5262–5275.

8 C. Wang, A. S. Batsanov, M. R. Bryce, S. Martín, R. J. Nichols, S. J. Higgins, V. M. García-Suárez and C. J. Lambert, *J. Am. Chem. Soc.*, 2009, **131**, 15647–15654.

9 V. M. García-Suárez and C. J. Lambert, *Nanotechnology*, 2008, **19**, 455203.

10 H. Sadeghi, S. Sangtarash and C. J. Lambert, *Nano Lett.*, 2015, **15**, 7467–7472.

11 D. Z. Manrique, C. Huang, M. Baghernejad, X. Zhao, O. A. Al-Owaedi, H. Sadeghi, V. Kaliginedi, W. Hong, M. Gulcur, T. Wandlowski, M. R. Bryce and C. J. Lambert, *Nat. Commun.*, 2015, **6**, 3689.

12 D. Z. Manrique, Q. Al-Galiby, W. Hong and C. J. Lambert, *Nano Lett.*, 2016, **16**, 1308–1316.

13 C. J. Lambert and S. X. Liu, *Chem. – Eur. J.*, 2018, **24**, 4193–4201.

14 E. Gorenskaia, M. Naher, L. Daukiya, S. Moggach, D. C. Milan, A. Vezzoli, C. Lambert, R. Nichols, T. Becker and P. J. Low, *Aust. J. Chem.*, 2021, **74**, 806–818.

15 M. Naher, E. Gorenskaia, S. A. Moggach, T. Becker, R. J. Nichols, C. J. Lambert and P. J. Low, *Aust. J. Chem.*, 2022, **75**, 506–522.

16 B. Xu and N. J. Tao, *Science*, 2003, **301**, 1221–1223.

17 N. R. Champness, A. N. Khlobystov, A. G. Majuga, M. Schröder and N. V. Zyk, *Tetrahedron Lett.*, 1999, **40**, 5413–5416.

18 M. Naher, S. Bock, Z. M. Langtry, K. M. O'Malley, A. N. Sobolev, B. W. Skelton, M. Korb and P. J. Low, *Organometallics*, 2020, **39**, 4667–4687.

19 P. Pachfule, A. Acharjya, J. Roeser, T. Langenhahn, M. Schwarze, R. Schomäcker, A. Thomas and J. Schmidt, *J. Am. Chem. Soc.*, 2018, **140**, 1423–1427.

20 A. G. L. Olive, K. Parkan, C. Givelet and J. Michl, *J. Am. Chem. Soc.*, 2011, **133**, 20108–20111.

21 L. Su, J. Dong, L. Liu, M. Sun, R. Qiu, Y. Zhou and S. F. Yin, *J. Am. Chem. Soc.*, 2016, **138**, 12348–12351.

22 D. C. Milan, A. Vezzoli, I. J. Planje and P. J. Low, *Dalton Trans.*, 2018, **47**, 14125–14138.

23 W. Y. Man, S. Bock, N. N. Zaitseva, M. I. Bruce and P. J. Low, *J. Organomet. Chem.*, 2011, **696**, 2172–2176.

24 K. West, C. Wang, A. S. Batsanov and M. R. Bryce, *J. Org. Chem.*, 2006, **71**, 8541–8544.

25 P. Moreno-García, M. Gulcur, D. Z. Manrique, T. Pope, W. Hong, V. Kaliginedi, C. Huang, A. S. Batsanov, M. R. Bryce, C. Lambert and T. Wandlowski, *J. Am. Chem. Soc.*, 2013, **135**, 12228–12240.

26 C. Li, I. Pobelov, T. Wandlowski, A. Bagrets, A. Arnold and F. Evers, *J. Am. Chem. Soc.*, 2008, **130**, 318–326.

27 T. Fu, K. Frommer, C. Nuckolls and L. Venkataraman, *J. Phys. Chem. Lett.*, 2021, **12**, 10802–10807.

28 W. Hong, D. Z. Manrique, P. Moreno-García, M. Gulcur, A. Mishchenko, C. J. Lambert, M. R. Bryce and T. Wandlowski, *J. Am. Chem. Soc.*, 2012, **134**, 2292–2304.

29 D. C. Milan, O. A. Al-Owaedi, M. C. Oerthel, S. Marqués-González, R. J. Brooke, M. R. Bryce, P. Cea, J. Ferrer, S. J. Higgins, C. J. Lambert, P. J. Low, D. Z. Manrique, S. Martin, R. J. Nichols, W. Schwarzacher and V. M. García-Suárez, *J. Phys. Chem. C*, 2016, **120**, 15666–15674.

30 L. Y. Zhang, P. Duan, J. Y. Wang, Q. C. Zhang and Z. N. Chen, *J. Phys. Chem. C*, 2019, **123**, 5282–5288.

31 Y. Zang, T. Fu, Q. Zou, F. Ng, H. Li, M. L. Steigerwald, C. Nuckolls and L. Venkataraman, *Nano Lett.*, 2020, **20**, 8415–8419.

32 M. Naher, D. C. Milan, O. A. Al-Owaedi, I. J. Planje, S. Bock, J. Hurtado-Gallego, P. Bastante, Z. M. A. Dawood, L. Rincón-García, G. Rubio-Bollinger, S. J. Higgins, N. Agraït, C. J. Lambert, R. J. Nichols and P. J. Low, *J. Am. Chem. Soc.*, 2021, **143**, 3817–3829.

33 E. J. Dell, B. Capozzi, K. H. Dubay, T. C. Berkelbach, J. R. Moreno, D. R. Reichman, L. Venkataraman and L. M. Campos, *J. Am. Chem. Soc.*, 2013, **135**, 11724–11727.

34 T. Fu, Y. Zang, Q. Zou, C. Nuckolls and L. Venkataraman, *Nano Lett.*, 2020, **20**, 3320–3325.

35 W. Lee, S. Louie, A. M. Evans, N. M. Orchanian, I. B. Stone, B. Zhang, Y. Wei, X. Roy, C. Nuckolls and L. Venkataraman, *Nano Lett.*, 2022, **22**, 4919–4924.

36 S. Li, H. Yu, J. Li, N. Angello, E. R. Jira, B. Li, M. D. Burke, J. S. Moore and C. M. Schroeder, *Nano Lett.*, 2021, **21**, 8340–8347.

37 L. Venkataraman, J. E. Klare, C. Nuckolls, M. S. Hybertsen and M. L. Steigerwald, *Nature*, 2006, **442**, 904–907.

38 M. Kamenetska, S. Y. Quek, A. C. Whalley, M. L. Steigerwald, H. J. Choi, S. G. Louie, C. Nuckolls, M. S. Hybertsen, J. B. Neaton and L. Venkataraman, *J. Am. Chem. Soc.*, 2010, **132**, 6817–6821.

39 O. Adak, R. Korytár, A. Y. Joe, F. Evers and L. Venkataraman, *Nano Lett.*, 2015, **15**, 3716–3722.

40 A. Borges, E. D. Fung, F. Ng, L. Venkataraman and G. C. Solomon, *J. Phys. Chem. Lett.*, 2016, **7**, 4825–4829.

41 S. Y. Quek, M. Kamenetska, M. L. Steigerwald, H. J. Choi, S. G. Louie, M. S. Hybertsen, J. B. Neaton and L. Venkataraman, *Nat. Nanotechnol.*, 2009, **4**, 230–234.

42 S. Chappell, C. Brooke, R. J. Nichols, L. J. Kershaw Cook, M. Halcrow, J. Ulstrup and S. J. Higgins, *Faraday Discuss.*, 2016, **193**, 113–131.

43 X. Zhao, C. Huang, M. Gulcur, A. S. Batsanov, M. Baghernejad, W. Hong, M. R. Bryce and T. Wandlowski, *Chem. Mater.*, 2013, **25**, 4340–4347.

44 L. Luo, S. H. Choi and C. D. Frisbie, *Chem. Mater.*, 2011, **23**, 631–645.